Intracellular Positioning Systems Limit the Entropic Eviction of Secondary Replicons Toward the Nucleoid Edges in Bacterial Cells

Julie Dauverd -Girault, Charlène Planchenault, Marine Pons, Caroline Schiavon, Patricia Siguier, Jérôme Rech, Catherine Guynet, Julie Dauverd-Girault, Jean Cury, Eduardo P C Rocha, et al.

Intracellular positioning systems limit the entropic eviction of secondary replicons toward the nucleoid edges in bacterial cells

Charlène Planchenault[1], Marine C. Pons[2], Caroline Schiavon[2], Patricia Siguier[2], Jérôme Rech[2], Catherine Guynet[2], Julie Dauverd – Girault [1], Jean Cury[3], Eduardo PC Rocha[3], Ivan Junier[4], François Cornet[2], Olivier Espéli[1]*

[1] Center for Interdisciplinary Research in Biology – Collège de France, CNRS UMR7241, INSERM U1050, PSL University

[2] Centre de Biologie Intégrative de Toulouse (CBI Toulouse), Laboratoire de Microbiologie et Génétique Moléculaires (LMGM), Université de Toulouse, UPS, CNRS, France.

[3] Microbial Evolutionary Genomics, Institut Pasteur, CNRS, UMR3525, Paris, France

[4] TIMC-IMAG, CNRS UMR5525 - Université Grenoble Alpes, Campus Santé - Institut Jean Roget

* to whom correspondence should be sent: olivier.espeli@college-de-france.fr

Abstract

Bacterial genomes, organized intracellularly as nucleoids, are composed of a main chromosome coexisting with different types of secondary replicons. Secondary replicons are major drivers of bacterial adaptation by gene exchange. They are highly diverse in type and size, ranging from less than 2 to more than 1000 kb, and must integrate with bacterial physiology, including to the nucleoid dynamics, to limit detrimental costs leading to their counter-selection. We show that large DNA circles, whether from a natural plasmid or excised from the chromosome tend to localize in a dynamic manner in a zone separating the nucleoid from the cytoplasm at the edge of the nucleoid. This localization is in good agreement with in silico simulations of DNA circles in the nucleoid volume. Subcellular positioning systems counteract this tendency, allowing replicons to enter the nucleoid space. In enterobacteria, these systems are found in replicons above 25 kb, defining the limit with small randomly segregated plasmids. Larger replicons carry at least one of the three described family of systems, ParAB, ParRM and StbA. Replicons above 180 kb all carry a ParAB system, suggesting this system is specifically required in the cases of large replicons. Simulations demonstrated that replicon size profoundly affects localization, compaction and dynamics of DNA circles in the nucleoid volume. The present work suggests that presence of partition systems on the larger plasmids or chromids is not only due to selection for accurate segregation but also to counteract their unmixing with the chromosome and consequent exclusion from the nucleoid.

Introduction

Bacterial genomes are compact and highly organized both at the genetic and physical levels. Genome organization results from the need of a compromise between folding chromosomes much longer than bacterial cells and favoring the interaction between DNA and machineries implicated in processes such as transcription, replication and segregation. Bacterial genomes are composed of one main chromosome and most often contain secondary replicons. Main chromosomes range from few hundred to over ten thousand kilobases (kb) and are the largest replicon in the cell. Secondary replicons comprise are highly variable in type and size (Smillie *et al*, 2010). It is generally admitted that they fall into three categories: small multicopy plasmids, larger low copy-number plasmids and chromids, also called secondary chromosomes that are large replicons (generally > 500 kb) found in genomes across a species (Harrison *et al*, 2010). Plasmids carry numerous adaptive functions, including numerous virulence factors, and are the major drivers of the transfer of antibiotic resistance genes. Although most plasmids are relatively small (less than 150 kb), they may together account for up to 30% of the genome. Chromids are frequent and appeared independently in several taxa. They originate from plasmids – from different plasmid families depending on species - as judged by the sequence of their replication origins (e.g. Ramachandran *et al*, 2017). Large plasmids and chromids often carry complex traits involved in bacteria-eukaryote interaction in infections and symbiosis processes (e.g. Marchetti *et al*, 2010). However, how and why some plasmids are domesticated as chromids is currently poorly understood.

Depending on the plasmid and its interaction with its genetic background, plasmids can be costly because of the metabolic burden imposed by plasmid replication, the consumption of resources for the expression of plasmid-encoded genes, synthesis of the plasmid conjugation apparatus, alteration in the expression of host genes or fine-tuning cellular pathways, and other metabolic effects such as the introduction of efflux pumps transporting important biomolecules (Baltrus, 2013). Incoming plasmids can be badly adapted to host physiology, imposing a high fitness cost that can be compensated by mutations in the plasmid and/or the host chromosome, rapidly selected for by their effect on growth (Carroll & Wong, 2018; Bouma & Lenski, 1988). How secondary replicons impact the global nucleoid dynamics at the cellular scale and has to adapt to it has received so far poor attention.

Small multicopy plasmids are thought to both replicate and segregate following a "random copy choice" model (Reyes-Lamothe *et al*, 2014; Wang, 2017). Other natural (non-engineered) bacterial plasmids are maintained at low copy numbers, rendering their maintenance by random segregation inefficient. These low copy number plasmids necessitate active systems to avoid loss during proliferation . Systems acting as poison-antidote (toxin/antitoxin or restriction/modification systems) enhance their persistence by killing plasmid-free cells (Zielenkiewicz & Cegłowski, 2001). Systems acting in active segregation (partition (Par) systems) reduce the rate of plasmid loss by thousand folds (Bouet & Funnell, 2019). Active plasmid segregation follows DNA replication and involves the separation and transportation of the two copies of the replicon in opposite directions along the longitudinal cell axis, ensuring every daughter cell receives at least one copy of the plasmid. Almost all Par systems identified to date consist of three components: a “centromere” cis-acting site, a centromere-binding protein and an NTPase (ATPase or GTPase). Another system acting on the subcellular positioning and the maintenance of some plasmids but consisting only of a cis-acting

element and a protein binding this element, StbA, has been described more recently (Guynet *et al*, 2011).

Numerous studies have reported the intracellular localization of plasmid DNA using FROS systems or fluorescent versions of their Par proteins. Small plasmids such as ColE1-type plasmids tend to form clusters at the nucleoid periphery (Reyes-Lamothe *et al*, 2014). In contrast, low copy number plasmids like F, P1, RK2 and R388 are preferentially found around mid- or quarter-cell positions, colocalized with the bacterial nucleoid (Gordon *et al*, 1997; Niki & Hiraga, 1997; Erdmann *et al*, 1999; Sengupta *et al*, 2010; Drew & Pogliano, 2011; Guynet *et al*, 2011). This depended on Par or StbA systems, confirming these systems act in the subcellular positioning of their replicons. Plasmids belonging to different families are nevertheless tethered to different sites within the cell, and segregate at different times relative to one another and to the bacterial cell cycle (Ho *et al*, 2002). vidences indicate that the bacterial chromosome, compacted as a nucleoid, contributes both passively (as the major structure occupying space inside a bacterial cell) and actively (as a support and/or matrix for plasmid movement) to plasmid partition mechanisms (Le Gall *et al*, 2016; Derman *et al*, 2008). The F, P1 and R388 plasmids devoid of their Par or StbA systems are excluded from the nucleoid space (Niki & Hiraga, 1997; Erdmann *et al*, 1999; Le Gall *et al*, 2016; Guynet *et al*, 2011). The reason why plasmids deleted for their partition system are excluded from the nucleoid is not understood.

In the present work we analyzed the completely sequenced genomes of enterobacteria to survey the presence of partition systems encoded by secondary replicons. We observed that partition systems are present in replicons with a characteristic size above 25kb, and lacking in smaller plasmids. We postulated therefore that the size of a plasmid is a critical determinant of its cost independently of the genes that it encodes. To experimentally test this hypothesis, we analyzed the localization, the dynamics and the loss frequency of the large R27 plasmid from which we perturbed the partition systems. As observed for other plasmids localization of the R27 plasmid in the nucleoid depends on a functional ParABS system, we therefore wanted to test if such nucleoid exclusion is not the default localization of circular DNA elements in *E. coli*. To test this hypothesis we monitored the localization of a large DNA circle excised from the chromosome and performed in silico simulation of polymer circles localization within nucleoid.

Our results indicate that the R27 plasmid lacking its ParAB system is more frequently localized towards the pole of the cell at the edge of the nucleoid. We observed a similar localization and mobility characteristics for large DNA circles excised from the chromosome. Simulations suggest that this polar exclusion can be explained by the sole force of entropic repulsion of the polymers. We observed that circles and plasmid do not occupy DNA free regions but rather localized at the transition between the cytoplasm and the nucleoid, suggesting that large DNA molecules do not get access easily to the cytoplasm of *E. coli*. Localization at the nucleoid – cytoplasm frontiers can be disadvantageous for various DNA metabolic processes such as replication, transcription or recombination that happen in the nucleoid core. This leads us to propose that, in addition to assist the correct segregation of replicated plasmids, partition systems have the function of targeting plasmids to the nucleoid. We further propose that this is advantageous for them.

Results

The size of the plasmid determines the presence and the type of partition systems

To study the distribution of subcellular positioning systems in secondary replicons, we selected 971 secondary replicons from sequenced Enterobacterial genomes (Table S1). These were representative of the different replicon families as judged by the genus they belong to (Table S2), the diversity of their replication origins and initiator proteins (Rep types) as well as their transfer functions (MOB types). They ranged from 1.3 to 794 kb in size and show a clear bimodal size distribution with a separation between peaks at around 25 kb (Figure 1).Twenty five percent of these plasmids were less than 25 kb and were predicted to have either a rolling-circle type or a theta type replication. These theta type small plasmids are supposed high copy number based on their described homologs. The repartition of sizes was then monotonous from 30 to 120 kb except for a large over-representation of 90 to 100 kb plasmids (11% of total); 23% were longer than 130 kb but only 1% were longer than 200 kb and 7 were chromids (> 500 kb). Very large secondary replicons are thus rare in Enterobacteria. We searched for three types of subcellular positioning / segregation systems: ParAB, ParRM and StbA (Figure 1). The well-described ParAB and ParRM systems were searched using appropriate HMM profiles (Table S1, text S1), (Cury *et al*, 2017)). The StbA protein, experimentally studied in R388, was first searched by similarity using the six *stbA* alleles previously identified (Guynet *et al*, 2011), a HMM profile was then constructed using the conserved N-terminal domains of the StbA homologs detected (Material and Methods). Figure 1 shows the presence of these three systems in plasmids ranked by the size of the latter. The vast majority of small plasmids lack any system (Table S3). In contrast, most larger plasmids and chromids possess at least one system. The transition between these two types of replicons occurs around 25 kb, consistent with the minimum of plasmid size distribution. The ParAB system was more frequent than the ParRM and StbA systems. Strikingly, all plasmids above 180 kb, including the chromids, had a ParAB homolog. StbA was mostly present in medium-sized plasmids (34-148 kb). ParRM systems were more evenly distributed than StbA. However, their occurrences in replicons above 180 kb were always accompanied by the presence of a ParAB system.

The more detailed analysis of the 79 plasmids longer than 25 kb and lacking partition systems revealed potential ParAB or ParMR systems that did not score well enough in the automatic annotation or contained frameshifts. Some of the latter may result from sequencing errors (60 plasmids, Sup Table 2). We found that many of the remaining large plasmids lacking partition systems contained ribosomal operons, were almost entirely composed of bacteriophages or mobile genetic elements. We concluded that: (i) partition systems are effectively essential for plasmids above 25kb long in Enterobacteria; (ii) a ParAB system is specifically required for plasmids above 180 kb, and this includes all the chromids.

Localisation and dynamics of the R27 megaplasmid strongly depends on ParAB but not on ParRM

The above data suggest that large plasmids specifically require a ParAB system for their maintenance. To study the role of ParAB in a large plasmid, we use R27, a 180 kb long natural IncHI2 plasmid carrying resistance to tetracycline (Taylor, 1983) . As all IncHI2 plasmids, R27 codes for both a ParAB and a ParRM system. Both systems were reported to be able to stabilize an unstable cloning vector and involved in R27 maintenance and subcellular positioning, although the ParAB system had a larger

effect (Lawley and Taylor, 2003). We first analyzed the R27 sequence and detected a toxin-antitoxin (TA) system not previously annotated, which may impair stability assays. This TA system was deleted and replaced by the *lacI* gene, allowing a colored detection of plasmid less colonies on agar plates in an otherwise Δ(*lacI*) strain. Using this system, we confirmed the previous findings on the role of the ParAB and ParRM systems on R27 maintenance (SupFig 1). R27Δ(TA) was stable over 60 generation of growth. Its Δ(*parAB*) derivative was lost whatever the growth conditions (L-broth or M9 broth supplemented with glycerol and casamino acids), although loss was more frequent during rapid growth (L-broth). This contrasted with the Δ(*parRM*) derivative, which was lost only during rapid growth. This confirms that ParAB is the prominent system for R27 stability.

When tagged with a FROS system, R27 derivatives were shown to localise plasmids (Lawley and Taylor, 2003). Single foci tended to localize close to mid-cell, whereas two or more foci localized symmetrically along cell length. These localizations depended on the ParAB system and to a lesser extent on the ParRM system. To further explore the role of the two Par systems, we tagged our R27 derivatives with a $parS_{P1}$ site and transfer them into strains producing a GFP-ParB fusion protein from a Δ(*lacZ*)::$gfp\text{-}parB_{P1}$ chromosomal construct (Stouf *et al*, 2013). R27Δ(TA) localized in the midcell zone when present as a single focus and towards the cell quarters in cells with two foci. The Δ(*parAB*) derivative do not present this localization whereas no defect was detectable for the Δ(*parRM*) derivative (Figure 1B - D). We thus confirm that R27 localizes as the smaller plasmids F, P1 and R388 plasmids, showing its large size does not preclude localization inside the nucleoid and that this effect depends on ParAB.

Taken together, our data suggest that large plasmids strictly need a ParAB system for their maintenance. ParAB maintain plasmid copies inside the nucleoid whatever their size, whereas ParRM systems don't. When devoid of ParAB systems, large plasmids exit the nucleoid and localize in a dynamic manner at the polar nucleoid edge. Localizing inside the nucleoid may thus be especially important for very large plasmids and chromids. To understand why this should be, we performed simulations of secondary replicon dynamics of different sizes.

Polymer modeling shows that plasmids are evicted from the nucleoid

In silico simulations of DNA and chromosome polymers have been extremely useful to evaluate physics of chromosome and plasmid conformation and segregation (Vologodskii & Cozzarelli, 1993; Vologodskii *et al*, 1992; Jun & Mulder, 2006; Junier *et al*, 2014). Monte Carlo simulations revealed that bacterial chromosomes unmix in the confined environment formed by the nucleoid shell (Jun & Mulder, 2006). We used simulations to evaluate if the localization and conformation of plasmids lacking partition systems was a consequence of entropy-mediated unmixing of polymers. We simulated a 3D nucleoid containing one chromosome and one plasmid over tens of millions of iterations (simulation steps). The nucleoid volume was defined by a cylinder with a long axis of 2000 nm and a diameter of 800 nm (Figure 2A). The chromosome was modeled using a 40 nm thick semi-flexible chain accounting for the nucleoprotein structure that has been observed in rapidly dividing cells with a 100bp/nm base-pair density along the main axis of the chain and a persistence length of 100 nm that is much smaller than the diameter of the nucleoid. In practice, the simulations were performed by discretizing the chromosome and plasmid chains using 30 nm long cylinders (1392 cylinders in total for the chromosome). Plasmid size was varied from 30 kb (9 cylinders) to 1400 kb

(423 cylinders). Finally, to quantify the impact of chromosome on the location properties of plasmids we used, as a control, simulations where only the plasmid was present in the nucleoid shell. Localizations of plasmids in the absence of a chromosome dramatically differed from that of plasmids evolving in a chromosome crowded nucleoid cell (Supplementary Figure S2 and S3).

We first quantified the localization of plasmids along the long axis of the nucleoid as a function of their size (L_p). Plasmids with less than 100 kb, localized at approximately similar frequencies inside and outside of the area defined by the chromosome edges, whereas large plasmids resided preferentially on the outside of the chromosome (Figure 2B and Figure 3A). Along the short axis of the nucleoid, the barycenter of small plasmids was found with equal probability on the edge or near the center of the nucleoid volume while the barycenter of large plasmid was mainly observed closer to nucleoid center (Figure 3A). This behavior was significantly different than what we observed for plasmid evolving in an empty nucleoid shell (Supplementary Figure S1). The results of these simulations are in good agreement with the polar localization observed for F (Le Gall *et al*, 2016) or R27 plasmids lacking a partition system (Figure 1B - D). This suggests that partition systems may counteract entropy mediated unmixing of plasmid and chromosomes and to allow plasmids to enter in the main nucleoid volume. Even if the unmixed state is frequent, we observed plasmids localized in between chromosome edges when they were traveling from one side to the other of the nucleoid (Figure 2B). Observation of few examples suggested that plasmid traveling across the nucleoid pass on the side of the chromosome (Figure 3B). To check how frequently plasmid and chromosome actually overlap, we measured the distance of the plasmid barycenter from the nucleoid center on the short cell axis as a function of their position along the long nucleoid axis (Figure 3C). We observed the same trend for small (100kb) and large (600kb) plasmids: when they localized over the chromosome on the long axis of the nucleoid, they were excluded from the nucleoid center on the short axes (Figure 3C). Interestingly, small plasmids were also pushed toward lateral edges of the nucleoid when at the pole, while large plasmids were not. This positioning was dramatically different in a chromosome free shell (Supplementary Figure S2). We conclude that plasmids and chromosomes are mostly unmixed whatever their size and position in the nucleoid.

The length of the plasmid determines its compaction within nucleoid

The simulations allowed us to question several aspects of the interplay between plasmids and the chromosome. First, we tested if plasmid and chromosome compaction was modulated by plasmid size. We used plasmid and chromosome spreading, i.e. the longitudinal or lateral extension of plasmids and chromosome as a proxy of their compaction within nucleoid. Our simulations were performed with a fixed nucleoid volume. First, plasmid spreading was measured along the short or the long axis of the nucleoid. Plasmid spreading was directly dependent on the size of the plasmid and the presence chromosomal DNA (Figure 4A and Supplementary Figure S2). Plasmid spreading decreased following a power law with plasmid size. Longitudinal chromosome spreading was only modestly affected by the presence of plasmid. Large plasmids (>1000 kb), however, imposed a reduction of the chromosome extension by 15% (Figure 4A). Interestingly, in the presence of the chromosome, plasmid compaction (the longitudinal spread of plasmid normalized by its size, NLS) was dramatically dependent on plasmid size. NLS follows a power law, $NLS = A * L_p^{-0.5}$, where L_p the length of the plasmid in kb and A the NLS value when L_p tends towards 0 (Figure 4B). Plasmids above

700 kb were compacted to the level of the chromosome while smaller plasmids were much less compacted (Figure 4B). For plasmids below 100 kb the compaction was not significantly changed by the presence of chromosome compared to the empty nucleoid shell (Figure 4B). These results suggest that if the nucleoid volume is maintained constant in the cell, plasmid larger than 100 kb will be compacted to fit in the nucleoid volume; this compaction will be severe for the largest plasmids.

Mobility of plasmid polymers

We observed plasmid trajectories crossing the nucleoid. Because Monte-Carlo simulations are dedicated (in principle) to quickly reach equilibrium, they may not be suitable for dynamical analyses. However, accepted motions in our model correspond to small, local deformations of the chain, and thus often provide a good estimation of the resulting large-scale dynamics of systems. Simulation traces show that plasmid localizations were highly similar between short interval iterations (, suggesting that localization at iteration N was not completely independent from the localization at iteration N-1. As a consequence, we can analyze plasmid trajectories. In this context, we first measured how frequently plasmids cross the chromosome territory along the long axis of the cell (Figure 4C). This parameter might be important when considering random segregation of plasmids without partition machinery. We observed that crossing frequency exponentially decayed with plasmid size. In the length of our simulations (>5e10^7 steps) plasmids above 1MB extremely rarely crossed the chromosome territory. When plasmids were smaller than 600 kb, both the frequency (Figure 4C) and the speed (Figure 4D) of crossing events were strongly dependent on their size. We measured the average velocity of nucleoid crossings in the 200 kb plasmid simulation and compared it to the reptation of an individual chromosomal locus (Figure 4E). Plasmid crossings were much faster than reptations of chromosomal loci. This suggests that unmixing of polymers is much more efficient than reptation inside a single polymer. Rapid unmixing has been already observed for 2 chromosome polymers of equal size (Jun & Mulder, 2006) but, to our knowledge, this was not described for two polymers of different sizes in a nucleoid like confinement. Finally, we measured mobility of plasmids at their polar position; it showed that mobility of small plasmids was higher than that of large plasmids and chromosome (Figure 4F). The velocity of plasmids that crossed the nucleoid (Figure 4E) was comparable (9 nm / 1000 iterations for a 200 kb plasmid) to that of plasmid at their polar home position (8.2 nm /1000 iterations for a 200 kb plasmid). Therefore during nucleoid crossing the directionality is imposed by a higher frequency of correlated movements but not by an acceleration (Figure 4E).

Localization of excised DNA circles is akin to the localization ofR27plasmids lacking the ParAB system

In the purpose to confirm R27 experiments and simulations with a heterologous system, we used an assay designed by F. Boccard and colleagues that allows excision of large DNA segments from the chromosome as DNA circles (Valens *et al*, 2016). The excised segment is tagged with a *parS*/parBGFP system to image its localization and dynamics. The strain also expresses a HupA-mCherry fusion to visualize the nucleoid. We have chosen to excise a 137 kb segment of the chromosome 400kb away from *oriC*. Before excision, this locus presented the typical patterns of localization of the *oriC* region,

cells with 2 to 4 foci localized at the quarters and 1/8 of the cell. Following induction of the recombinase for 30 min (a sufficient induction to nearly reach 100% of excision) the localization of the ParB-GFP foci dramatically changed, most cells presented one focus localized at the edge or at the middle of the nucleoid (Figure 5A). This polar localization is akin to the localization observed with the R27 plasmid lacking the partition system. The frequency of polar foci was higher for the excised circles (75%) compared to the R27 plasmid lacking ParAB system (35%), suggesting that R27 Δ*parAB* keeps some nucleoid targeting elements, may be the ParRM system. These results demonstrate that DNA circles lacking positioning system tend to be positioned at the nucleoid edge.

Long range movements of R27 and excised DNA circles

We used time lapse microscopy to evaluate the mobility of the excised circle and R27 plasmid (Figure 5B). Kymographs of plasmid lacking ParAB and excised foci differed significantly from that of chromosomal foci (Figure 5B). At long time scale (2h with 10 min intervals) we observed, with the excised circles and the R27Δ*parAB* plasmid, frequent long, rapid and oriented movements. These movements frequently produced merging of foci (Figure 5B). These movements consisted in foci moving from the nucleoid toward the cell pole or toward the nucleoid free mid-cell zone (Figure 5C). Chromosomal loci also presented ballistic like movements but they mainly corresponded to segregation events and they were confined to the nucleoid area. We measured that average velocity of ballistic movements of excised circles and chromosomal loci segregating. Velocity of nucleoid crossing by excised circles toward cell pole is 142 +/- 80 $nm.min^{-1}$ (N=50), this is 3 times faster than the average velocity of chromosomal loci segregating from quarter positions, 50 +/- 30 $nm.min^{-1}$ (N=50). Using the same localization system, P. Wiggins and colleagues observed that most chromosomal loci present a maximal drift velocity, ≈ 300 $nm.min^{-1}$, immediately after foci splitting (Cass *et al*, 2016). Two minutes later drift velocity has already slowed down to 20 - 50 $nm.min^{-1}$ to finish segregation in 20 min. Here we observed prolonged high velocity movements of excised circles, they might correspond to the ballistic movements observed in the simulation; therefore they can give an estimation of the efficiency of entropy mediated unmixing in these experimental conditions.

Dynamics of R27 and excised DNA circles

At shorter time scale (3 min with 6 sec intervals) ballistic movements of chromosomal loci, R27 or excised circles were rarely detected (Figure 5B). After reaching the nucleoid edges, excised circles and R27 plasmid lacking the ParAB system unfrequently escaped from this positioning. By contrast we observed significant longitudinal movement of the R27 and chromosomal locus (Figure 5B). We measured Mean Squared Displacement (MSD) to obtain quantitative analysis of the mobility of foci (Figure 5D - G). MSD curves were characteristic of subdiffusive motions, following a power law: $MSD = D*\Delta T^{\alpha}$ where D is coefficient of diffusion, ΔT the time interval and α the scaling exponent. MSD confirmed that excised foci present a different mobility compared to chromosomal loci (Figure 5D and 5E). For time intervals around 2 sec, the MSD α coefficient of excised foci (0.43) is reduced compared to chromosomal foci (0.48). The coefficient of diffusion is of excised foci is also reduced (0.0044 vs 0.0053 $\mu m^2 .sec^{-1}$). The cage surrounding the movements of excised foci is also reduced by a factor of 2. Finally, the average distance that excised foci travel in one interval is 20 % reduced compared to the chromosomal foci. Mobility of WT R27 plasmid (α = 0.66 and D = 0.0026 $\mu m^2 .sec^{-1}$ differed from that chromosomal loci or excised circles, Figure 5F and 5G). The absence of the ParAB system dramatically reduces the mobility of R27. It was particularly striking for the coefficient of

diffusion that dropped to 0.001 μm^2 $.sec^{-1}$. Our observations demonstrate, for every dynamics parameters, that R27 plasmid lacking ParAB behavior is akin but not strictly identical to the excised circle.

Nucleoid edges serves as a platform for DNA circle surfing

Differently from the simulations we observed that plasmids lacking partition systems and excised circles were less mobile than chromosomal loci. This suggests that the nucleoid edge is not a constrain-free localization. To understand what is constraining the mobility of excised circles and plasmids at the nucleoid edges, we investigated this localization in more details. Fluorescence quantification suggested that excised circle foci localized precisely at the edges of the nucleoid but do not freely navigate in the DNA free zone at the pole of cell (Figure 6A). As illustrated for one example, we frequently observed, for excised loci, that mobility along the short axis of the cell is higher compared to mobility along the long axis of the cell (Figure 6B). We deconvoluted and performed a three dimensional reconstruction of the Z stack over time (see material and methods) to evaluate the dynamics of these foci at the nucleoid edge, we observed that excised foci moved rapidly on the surface of the nucleoid but keep nucleoid contact for most of their moves (Figure 6C). Deconvolution process allowed the transient resolution of 2 foci at the nucleoid edge, confirming that polar foci are frequently clusters of two or more excised circles. These results suggest that large DNA circles and plasmids lacking partition systems are expelled from the nucleoid core, in agreement with our simulations, and find a home position at the nucleoid edge where they are free to surf on the nucleoid surface but cannot escape it. Excised circles might be unmixed from the nucleoid on the sole force of entropy but concomitantly they are maintained at the transition between the DNA compartment and the cytoplasm.

Localization and dynamics of R27 plasmid and excised circles when nucleoid and cell organization are perturbed

Finally we tested if R27 and the excised DNA circle localizations at the nucleoid edge were maintained when chromosome confinement was changed. First, we used chloramphenicol to condense the nucleoid immediately after excision. We observed profound changes in the localization and dynamics of excised foci in these conditions (Figure 6D and 6E). The number of circle foci increased significantly (2 to 3 per cell compared to 1 to 2 in the regular condition). The localization of these foci was changed, they were not only localized to the edge of the nucleoid, they were also observed on the side of the nucleoid. Even if the DNA free zone at the pole of the cell was enlarged by chloramphenicol treatment the excised circles did not explore it, they always kept contact with the nucleoid. Time-lapse experiments revealed that excised circle foci travel from the edge to the side of the nucleoid and vice versa (Figure 6E). In the presence of chloramphenicol, R27 plasmid localized to the side of the nucleoid and did not explore nucleoid free regions (Figure 6F). Similar results were observed with WT and Δ*parAB* plasmids suggesting that chloramphenicol is altering the ParAB positioning system. These observations suggest that localization at the nucleoid pole is dependent on the volume occupied by the nucleoid or might eventually be created by transcription-translation-secretion (transertion) barriers (Roggiani & Goulian, 2015). We used cephalexin to block

cell division and create large DNA free zones between segregated nucleoids. In these conditions filamenting cells presented multiple foci on the edge, the side and on the nucleoid (Figure 6G). The nucleoid-foci association was maintained for most cells. We only observed one focus crossing a nucleoid free space out of 200 cells monitored by time lapse over a 2h period (Figure 6G, right panel). We tested the impact of transcription inhibition by rifampicin (Figure 6H); this antibiotic has for consequence to expand the nucleoid. In the presence of rifampicin, we observed foci of the excised region at the edges of the nucleoid. These polar foci were frequently fuzzier than the one observed in regular conditions. Time lapse imaging revealed that they corresponded to 2 - 3 excised circles that cohabited in the same region of the cell but did not overlap completely as frequently than in the absence of the drug (Figure 6I). These results confirmed that DNA circles lacking a partition system are unmixed from the chromosome but are maintained in the nucleoid space at the transition between the nucleoid and the cytoplasm.

Discussion

Partition machinery and localization of plasmid

Our work extends to R27 the observation that plasmid lacking partition system are not localized with the nucleoid core. Using excised chromosomal circles and simulation we confirmed that this localization relies on the biophysical nature of large DNA circles in a crowded nucleoid and cytoplasm environment. Since the “natural” positioning of plasmids lacking partition systems is on the edge of the nucleoid, one could ask why partition systems do target plasmids inside the nucleoid? What could be the benefit for plasmid segregation to happen within the nucleoid? Could plasmid hijack entropy? In this scenario partition systems might serve as a localization system to the nucleoid to allow the plasmid to benefit from the entropic flow. Directionality will be given by protein-protein interactions and reaction-diffusion process of the ParB and ParA ATPase (Walter *et al*, 2017).

How much plasmid DNA can be hosted in the nucleoid ?

Simulations indicate that for a define nucleoid volume the carrying capacity of plasmid DNA in the presence of a chromosome is limited. With the simulation parameters that we used, the normalized longitudinal spread of 700 kb plasmid reached that of the chromosome (Figure 5B). This limit is also observable in the frequency of nucleoid crossing that is extremely rare above 700 kb (Figure 6A). Above this size the plasmid, the nucleoid and perhaps cell morphology must adapt to this foreign DNA. Obviously this threshold is strictly dependent on the parameters that we used to define the polymers. Changing the persistence length, the diameter of the chromatin cylinders or the nucleoid volume will modify these limits. Nevertheless, it is tempting to compare this 700 kb threshold with the size of plasmid and secondary chromosomes observed in bacteria. Secondary replicons above 700 kb are secondary chromosomes. The presence of a large secondary replicon will therefore necessitate important chromosome conformation changes. Such changes could be detrimental and add an extra cost, in addition to the cost for replication and transcription, to secondary large replicons. Alternatively, the nucleoid volume might change to accommodate the extra replicon but this also has a significant cost in term of cell elongation for example.

The second critical size that we observed is much lower, under 200kb the probability to observe plasmid crossing the chromosome increased dramatically and the spread of plasmids approximate the values observed for plasmid residing in a chromosome free nucleoid shell. It is tempting to compare these values with the presence of segregation machinery encoded by plasmid genomes. Plasmids below 25-30 kb can cross the chromosome frequently and rapidly, ensuring efficient segregation by random partition. Above this value, the mobility of replicons becomes limiting and decrease exponentially with increasing size, rendering the presence of a positioning system required for stability. Above 200 kb, both the probability of crossing the chromosome and the crossing speed become extremely low, rendering compulsory the presence of a ParAB system, which is the only one of the three types of positioning systems ensuring both positioning of the replicons inside the nucleoid and separation of their sister copies after replication. Lastly, the presence of replicons above 700 kb in the nucleoid impact chromosome dynamics. These large replicons must thus adopt chromosome like behaviors. Consistent with this, the chromid of *V. cholerae* has an accurately regulated timing of replication, spreads in the long cell axis and couples segregation of its *ter* region with cell division as chromosomes do.

Plasmid and excised circles are maintained at the nucleoid –cytoplasm transition

We observed that large plasmids and DNA circles lacking partition systems were expulsed from their original localization toward nucleoid edges but did not invade the cytoplasmic space. This is in good agreement with our simulations suggesting that expulsion relates to entropic mediated unmixing of polymers in a confined space. However, entropy does not explain why these molecules do not invade large nucleoid free regions at the pole of the cell or in between nucleoids of filaments. One possible explanation for this could be that large circular DNA, differently, from small plasmid cannot diffuse in a glass-like cytoplasm (Parry *et al*, 2014). This has already been observed for other type of cytoplasm components that become disproportionally constrained with increasing size. Remarkably, small plasmids lacking partition system appeared to diffuse rapidly within cytoplasm even when they form clusters (Reyes-Lamothe *et al*, 2014). A systematic analysis of plasmid or DNA circles mobility as a function of their size would be required to determine the critical size. However, we observed that DNA circles can slide rapidly on the surface of the nucleoid, this might suggest that the nature of the cytoplasm is not the only element contributing to their localization. Nucleic acid charges may also contribute to the control of diffusion at the transition between nucleoid and cytoplasm. Negatively charged ribosome surfaces may impose this limitation on the diffusion of proteins and DNA (Schavemaker *et al*, 2017). Interestingly the fluidity of the cytoplasm can be modulated by drugs affecting metabolism (Parry *et al*, 2014) or antimicrobial peptides (Zhu *et al*, 2019), our results suggest that plasmid localization and dynamics might also be affected by environmental conditions, this would influence their stability and expression and eventually change their cost for the host cell.

Could partition of genetic material imposes constrains on genome dynamics.

In bacteria, horizontal gene transfer (HGT) is the main source of genome dynamics. Recent studies revealed that the size of horizontally acquired DNA in one single event is limited to 25-30kb (Pang & Lercher, 2017, 2019). Plasmids and lysogenic phages are the main drivers of HGT. Interestingly this 25 kb limit also corresponds to the presence of partition systems on plasmids. Our simulations show that the ability of plasmid to cross the nucleoid is exponentially decreasing with increasing size

(Figure 5). Experiment with R27 plasmid or excised circles clearly show that nucleoid crossing is very rare for 130 kb -200 kb DNA circles. Entropic unmixing might therefore limit the ability of a newly acquired replicon to find a target sequence for integration. In good agreement with this hypothesis it appeared that DNA internal motion likely accelerates protein target search in a packed nucleoid (Chow & Skolnick, 2017)

Material and methods

Annotation of subcellular positioning systems

Partition systems ParAB and ParMR were detected using HMM profiles used in our previous work (Cury *et al*, 2017). Briefly, systems were reported when the two hits of a given system were contiguous in the replicon. A hit was considered significant if the e-value was smaller than 10^{-3} and the coverage of the profile was above 50%. For annotation of *stbA*, tBLASTN searches were first performed against the 971 plasmids using the *stbA* sequences previously reported (Guynet et al, 2011). Each plasmid with a positive result was annotated in SnapGene. oriTDB (http://202.120.12.134/oriTfinder/oriTfinder.html) was used to determine possible *oriT* site, relaxases and type IV secretion system genes. We found a stbA or stbA like sequence in 136 plasmids. A HMM profile was then constructed using the conserved N-terminal domains of the StbA homologs and used to search again the whole plasmid collection (Figure 1A). To further annotate plasmids with no detected systems, *parA* and *parM* genes were searched using tBLASTN in the 79 plasmids without any segregation system found. We used the *parA* sequence found in NC_012961, the *parM* sequences described by Jakob Møller-Jensen and colleagues (van den Ent *et al*, 2002) and the *parM* sequence of JCW3 (*Clostridium perfringens*). Using this strategy, we found 54 plasmids with a *parA-like* sequence (including 5 with a frameshift and 1 partial sequence) and 6 plasmids with *parM*-like sequence (including 3 with a frameshift). The 19 remaining plasmid sequences with no system detected were all annotated in SnapGene and inspected “by eyes”. Two sequences were obviously partial sequences of larger plasmids. Mobile genetics elements (MGE) were annotated using ISfinder (https://www-is.biotoul.fr//)(Siguier *et al*, 2006), bacteriophage with PHASTER (http://phaster.ca/) (Arndt *et al*, 2016). Four plasmids carried ribosomal operons, others were mostly constituted by MGE or bacteriophages.

Strains and plasmids

R27 is a 180 kb plasmid of the IncHI family, naturally resistant to tetracycline (Phan & Wain, 2008; Lawley & Taylor, 2003). We detected a potential toxin-antitoxin system consisting of gene *stm* and an upstream RNA, which we deleted from positions 91,174 to 91,481 bp on the R27 sequence and replaced by the *lacI* gene. For intracellular localization, we inserted a P1 *parS*-Kn cassette (Stouf *et al*, 2013) in the intergenic region between the two converging genes R149 and R150 (position 138,435). The ParAB and ParRM systems (R0019-R0020 and R0013-StbA, respectively) were deleted from the beginning of the first gene to the end of the second gene (23,081 to 25,338 and 18,079 to 19,834, repectively), replaced by a FRT-Kn-FRT cassette that was subsequently resolved to remove the KnR determinant. Note that the ParM homolog is called StbA in R27 annotation but is not a StbA homolog. R27 derivatives were introduced into a Δ(*lacI*) strain (Deghorain *et al*, 2011) for stability assays and in a Δ(*lacZ*)::*gfp-parBP1* strain (Stouf *et al*, 2013) for microscopy. For the excision of the

137 kb we used the FBG150 *trkD*^{attL} R719 strain (Valens *et al*, 2016) containing attL from λ at the *trkD* locus (3928826 bp) and *attR* at the position 4067141bp. Excision is produced by the Int and Xis protein from l produced from the plasmid pTSA29-CXI (Valens *et al*, 2004). The *parS* P1 tag was inserted at the Ori-7 position at 4024865 bp.

Imaging of excised DNA circle and R27. Excision was obtained as described before (Valens *et al*, 2016) with a 30 min heat shock at O.D. 0.1. Bacteria were immediately spread on M9-casaminoacids and glucose agarose pad supplemented or not with chloramphenicol (30 µg/ml) or rifampicin (50 µg/ml). When required, cephalexin (20µg/ml) was added to the culture medium 1 h before heat shock. Imaging was performed on a Zeiss inverted microscope equipped with a Yokogawa W1 spinning disk head and an Orca-Flash 4 CMOS camera. The incubation is maintained to 30°C during imaging. Time-lapse acquisition was controlled by Metamorph software. Deconvolution was performed with Huygens and 3D reconstruction with Imaris softwares. Image analysis was performed with Object J (Vischer *et al*, 2015), Microbe-J (Ducret *et al*, 2016), Track-mate (Tinevez *et al*, 2017) and Particle Tracker (Sbalzarini & Koumoutsakos, 2005).

Simulations. We simulated *E. coli* chromosomes using a worm-like chain (WLC) model, i.e. a flexible fiber model, of the bacterial chromosome (Junier *et al*, 2014; Lepage & Junier, 2017). One chromosomes and one plasmid were embedded in a volume whose dimensions corresponded to the nucleoid that is observed *in vivo*: a diameter equal to 800 nm and a length from 2.0 µm (G1 phase). We excluded the possibility of the fibers to overlap (self-avoidance constraint) by using hard-core diameters of the nucleoproteic fiber of 35 nm. The base-pair density along the fiber was fixed at 100 bp/nm and the persistence length at 100 nm, a value that is much smaller than the diameter of the nucleoid. Simulations and thermodynamic analysis were performed as described previously (Junier *et al*, 2014). Briefly the chromosome and plasmid consisted of a semi-flexible polymer composed of a succession of *N* impenetrable cylinders (three cylinders per persistence length)—*N* = 1392 for the 4.6 Mb chromosome. The state space of our polymer models was sampled using a standard Monte–Carlo procedure (Metropolis accept/rejection rule). For each plasmid we performed three simulations (two in the presence of the chromosome and one in its absence). Each simulation consisted of two stages: (i) an initialization stage (see above) and (ii) a thermodynamic analysis. The initial polymer conformations were obtained by first equilibrating the system in the presence of all forces and without confinement (large initial embedding volume). The cell volume was next slowly reduced down to the nucleoid volume, and the thermodynamic properties were eventually computed. The slow reduction of the embedding volume aimed at ensuring that the conformations were the most likely from a thermodynamic point of view (by preventing as much as possible the formation of long-living metastable kinetic conformations). The X, Y, Z position of each plasmid and chromosome monomer and the barycenter of the replicon were recorded every 15 000 iterations (Figure 2A).

Acknowledgements

We thank Stephane Duigou, Michele Valens and Frédéric Boccard for the gift of strains and technical advices for DNA excisions. We thank members of Orion, the CIRB imaging facility. We are deeply thankful to Thibault Lepage for his help on setting up the simulations. This work as funded by ANR

ANR-14-CE10-0007-01 to OE, FC and ER by the CNRS PICS initiative to OE and IJ and by the Foundation ARC (PJA 20171206119) to OE.

References

Arndt D, Grant JR, Marcu A, Sajed T, Pon A, Liang Y & Wishart DS (2016) PHASTER: a better, faster version of the PHAST phage search tool. *Nucleic Acids Res.* **44:** W16-21

Baltrus DA (2013) Exploring the costs of horizontal gene transfer. *Trends Ecol. Evol.* **28:** 489–495

Bouet J-Y & Funnell BE (2019) Plasmid Localization and Partition in Enterobacteriaceae. *EcoSal Plus* **8:**

Bouma JE & Lenski RE (1988) Evolution of a bacteria/plasmid association. *Nature* **335:** 351–352

Carroll AC & Wong A (2018) Plasmid persistence: costs, benefits, and the plasmid paradox. *Can. J. Microbiol.* **64:** 293–304

Cass JA, Kuwada NJ, Traxler B & Wiggins PA (2016) Escherichia coli Chromosomal Loci Segregate from Midcell with Universal Dynamics. *Biophys. J.* **110:** 2597–2609

Chow E & Skolnick J (2017) DNA Internal Motion Likely Accelerates Protein Target Search in a Packed Nucleoid. *Biophys. J.* **112:** 2261–2270

Cury J, Touchon M & Rocha EPC (2017) Integrative and conjugative elements and their hosts: composition, distribution and organization. *Nucleic Acids Res.* **45:** 8943–8956

Deghorain M, Pagès C, Meile J-C, Stouf M, Capiaux H, Mercier R, Lesterlin C, Hallet B & Cornet F (2011) A defined terminal region of the E. coli chromosome shows late segregation and high FtsK activity. *PloS One* **6:** e22164

Derman AI, Lim-Fong G & Pogliano J (2008) Intracellular mobility of plasmid DNA is limited by the ParA family of partitioning systems. *Mol. Microbiol.* **67:** 935–946

Drew KRP & Pogliano J (2011) Dynamic instability-driven centering/segregating mechanism in bacteria. *Proc. Natl. Acad. Sci. U. S. A.* **108:** 11075–11080

Ducret A, Quardokus EM & Brun YV (2016) MicrobeJ, a tool for high throughput bacterial cell detection and quantitative analysis. *Nat. Microbiol.* **1:** 16077

van den Ent F, Møller-Jensen J, Amos LA, Gerdes K & Löwe J (2002) F-actin-like filaments formed by plasmid segregation protein ParM. *EMBO J.* **21:** 6935–6943

Erdmann N, Petroff T & Funnell BE (1999) Intracellular localization of P1 ParB protein depends on ParA and parS. *Proc. Natl. Acad. Sci. U. S. A.* **96:** 14905–14910

Gordon GS, Sitnikov D, Webb CD, Teleman A, Straight A, Losick R, Murray AW & Wright A (1997) Chromosome and low copy plasmid segregation in E. coli: visual evidence for distinct mechanisms. *Cell* **90:** 1113–1121

Guynet C, Cuevas A, Moncalián G & de la Cruz F (2011) The stb operon balances the requirements for vegetative stability and conjugative transfer of plasmid R388. *PLoS Genet.* **7:** e1002073

Harrison PW, Lower RPJ, Kim NKD & Young JPW (2010) Introducing the bacterial 'chromid': not a chromosome, not a plasmid. *Trends Microbiol.* **18:** 141–148

Ho TQ, Zhong Z, Aung S & Pogliano J (2002) Compatible bacterial plasmids are targeted to independent cellular locations in Escherichia coli. *EMBO J.* **21:** 1864–1872

Jun S & Mulder B (2006) Entropy-driven spatial organization of highly confined polymers: Lessons for the bacterial chromosome. *Proc. Natl. Acad. Sci.* **103:** 12388–12393

Junier I, Boccard F & Espéli O (2014) Polymer modeling of the E. coli genome reveals the involvement of locus positioning and macrodomain structuring for the control of chromosome conformation and segregation. *Nucleic Acids Res.* **42:** 1461–1473

Lawley TD & Taylor DE (2003) Characterization of the double-partitioning modules of R27: correlating plasmid stability with plasmid localization. *J. Bacteriol.* **185:** 3060–3067

Le Gall A, Cattoni DI, Guilhas B, Mathieu-Demazière C, Oudjedi L, Fiche J-B, Rech J, Abrahamsson S, Murray H, Bouet J-Y & Nollmann M (2016) Bacterial partition complexes segregate within the volume of the nucleoid. *Nat. Commun.* **7:** 12107

Lepage T & Junier I (2017) Modeling Bacterial DNA: Simulation of Self-Avoiding Supercoiled Worm-Like Chains Including Structural Transitions of the Helix. *Methods Mol. Biol. Clifton NJ* **1624:** 323–337

Marchetti M, Capela D, Glew M, Cruveiller S, Chane-Woon-Ming B, Gris C, Timmers T, Poinsot V, Gilbert LB, Heeb P, Médigue C, Batut J & Masson-Boivin C (2010) Experimental evolution of a plant pathogen into a legume symbiont. *PLoS Biol.* **8:** e1000280

Niki H & Hiraga S (1997) Subcellular distribution of actively partitioning F plasmid during the cell division cycle in E. coli. *Cell* **90:** 951–957

Pang TY & Lercher MJ (2017) Supra-operonic clusters of functionally related genes (SOCs) are a source of horizontal gene co-transfers. *Sci. Rep.* **7:** 40294

Pang TY & Lercher MJ (2019) Each of 3,323 metabolic innovations in the evolution of E. coli arose through the horizontal transfer of a single DNA segment. *Proc. Natl. Acad. Sci. U. S. A.* **116:** 187–192

Parry BR, Surovtsev IV, Cabeen MT, O'Hern CS, Dufresne ER & Jacobs-Wagner C (2014) The bacterial cytoplasm has glass-like properties and is fluidized by metabolic activity. *Cell* **156:** 183–194

Phan M-D & Wain J (2008) IncHI plasmids, a dynamic link between resistance and pathogenicity. *J. Infect. Dev. Ctries.* **2:** 272–278

Ramachandran R, Jha J, Paulsson J & Chattoraj D (2017) Random versus Cell Cycle-Regulated Replication Initiation in Bacteria: Insights from Studying Vibrio cholerae Chromosome 2. *Microbiol. Mol. Biol. Rev. MMBR* **81:**

Reyes-Lamothe R, Tran T, Meas D, Lee L, Li AM, Sherratt DJ & Tolmasky ME (2014) High-copy bacterial plasmids diffuse in the nucleoid-free space, replicate stochastically and are randomly partitioned at cell division. *Nucleic Acids Res.* **42:** 1042–1051

Roggiani M & Goulian M (2015) Chromosome-Membrane Interactions in Bacteria. *Annu. Rev. Genet.* **49:** 115–129

Sbalzarini IF & Koumoutsakos P (2005) Feature point tracking and trajectory analysis for video imaging in cell biology. *J. Struct. Biol.* **151:** 182–195

Schavemaker PE, Śmigiel WM & Poolman B (2017) Ribosome surface properties may impose limits on the nature of the cytoplasmic proteome. *eLife* **6:**

Sengupta M, Nielsen HJ, Youngren B & Austin S (2010) P1 plasmid segregation: accurate redistribution by dynamic plasmid pairing and separation. *J. Bacteriol.* **192:** 1175–1183

Siguier P, Perochon J, Lestrade L, Mahillon J & Chandler M (2006) ISfinder: the reference centre for bacterial insertion sequences. *Nucleic Acids Res.* **34:** D32-36

Smillie C, Garcillán-Barcia MP, Francia MV, Rocha EPC & de la Cruz F (2010) Mobility of plasmids. *Microbiol. Mol. Biol. Rev. MMBR* **74:** 434–452

Stouf M, Meile J-C & Cornet F (2013) FtsK actively segregates sister chromosomes in Escherichia coli. *Proc. Natl. Acad. Sci. U. S. A.* **110:** 11157–11162

Taylor DE (1983) Transfer-defective and tetracycline-sensitive mutants of the incompatibility group HI plasmid R27 generated by insertion of transposon 7. *Plasmid* **9:** 227–239

Tinevez J-Y, Perry N, Schindelin J, Hoopes GM, Reynolds GD, Laplantine E, Bednarek SY, Shorte SL & Eliceiri KW (2017) TrackMate: An open and extensible platform for single-particle tracking. *Methods San Diego Calif* **115:** 80–90

Valens M, Penaud S, Rossignol M, Cornet F & Boccard F (2004) Macrodomain organization of the Escherichia coli chromosome. *EMBO J.* **23:** 4330–4341

Valens M, Thiel A & Boccard F (2016) The MaoP/maoS Site-Specific System Organizes the Ori Region of the E. coli Chromosome into a Macrodomain. *PLoS Genet.* **12:** e1006309

Vischer NOE, Verheul J, Postma M, van den Berg van Saparoea B, Galli E, Natale P, Gerdes K, Luirink J, Vollmer W, Vicente M & den Blaauwen T (2015) Cell age dependent concentration of Escherichia coli divisome proteins analyzed with ImageJ and ObjectJ. *Front. Microbiol.* **6:** 586

Vologodskii AV & Cozzarelli NR (1993) Monte Carlo analysis of the conformation of DNA catenanes. *J. Mol. Biol.* **232:** 1130–1140

Vologodskii AV, Levene SD, Klenin KV, Frank-Kamenetskii M & Cozzarelli NR (1992) Conformational and thermodynamic properties of supercoiled DNA. *J. Mol. Biol.* **227:** 1224–1243

Walter J-C, Dorignac J, Lorman V, Rech J, Bouet J-Y, Nollmann M, Palmeri J, Parmeggiani A & Geniet F (2017) Surfing on Protein Waves: Proteophoresis as a Mechanism for Bacterial Genome Partitioning. *Phys. Rev. Lett.* **119:** 028101

Wang Y (2017) Spatial distribution of high copy number plasmids in bacteria. *Plasmid* **91:** 2–8

Zhu Y, Mohapatra S & Weisshaar JC (2019) Rigidification of the Escherichia coli cytoplasm by the human antimicrobial peptide LL-37 revealed by superresolution fluorescence microscopy. *Proc. Natl. Acad. Sci. U. S. A.* **116:** 1017–1026

Zielenkiewicz U & Cegłowski P (2001) Mechanisms of plasmid stable maintenance with special focus on plasmid addiction systems. *Acta Biochim. Pol.* **48:** 1003–1023

Legend of the figures

Figure 1. A) Distribution of subcellular positioning systems in enterobacterial secondary replicons. 970 replicons were ranked according to their size (x-axis; the top panel shows a cumulative plot of replicon sizes indicative of size density). The bottom four panels show event plots of the presence of the indicated system (vertical line) or absence of system detected (none). B) Localization of the R27, R27 ΔparAB, R27 ΔparRM plasmids (*parS* /parBGFP, green) and nucleoid (Hu-mCherry, red) C) Localization along the long axis of the *E. coli* cell of the R27 tagged with a *parS* /ParB-GFP tag. Cells with one focus of the WT R27, R27 delta parAB, R27 delta parRM (N =1000). D) Distribution of R27 localization as in C for cells with two R27 foci.

Figure 2. A) Description of the in silico simulation of plasmid and chromosome and the main parameters that we collected during the simulations. B) In silico simulation of the localization pattern of plasmids (green circles) and chromosome edges (red traces) along the longitudinal axis of the nucleoid . Plasmid size (Lp) ranging from 30 kb to 1000 kb are represented. The simulations were run for at least $3x10^7$ iterations.

Figure 3. A) In silico simulations of the localization of plasmid barycenter along the longitudinal axis of the nucleoid (histograms) and the short axes of the nucleoid (scatter plot). The barycenter of the chromosome is plotted in red on the scatter plots. The black ovoid line map the position of the 70 kb plasmid the most distant from the cell center, the same line is drawn on the 600kb scatter plot to illustrate the fact that barycenters of large plasmids are more frequently localized toward nucleoid center. B) Examples of 600 kb plasmid (green polymer) localization according to the positioning of its barycenter along the longitudinal axis of the nucleoid. Plasmids crossing chromosomes (purple polymer) tend to occupy the lateral side of the nucleoid. C) Histograms of the localization of 200 kb and 600kb plasmid barycenters.

Figure 4. A) Analyzes of plasmid and chromosome spatial extension along the longitudinal axis (Zspread) of the cell. Red circle represent the median chromosome extension according to the size of the plasmid present in the same nucleoid. The green circles represent the extension of the plasmid in the presence of a chromosome. Open green circles represent the extension of plasmid in an empty nucleoid shell. Data were fitted with power laws. B) Normalized spreading (NS) of plasmids and chromosome along the longitudinal axis of the nucleoid. NS = Zspread / Size of the replicon (kb). Data were fitted with power laws. C) Frequency of plasmid crossing events according to plasmid size. Data were fitted by a double exponential decay [Freq crossing] = $25*e^{(-0.03*Lp)} + 9*e^{(-0.004*Lp)}$; R^2 =0.98. D) Average speed of chromosome crossing for small plasmids. Data were fitted by a double exponential decay [Crossing speed] = $1822*e^{(-0.15*Lp)} + 12*e^{(-0.007*Lp)}$; R^2 =0.99. E) Traces of the 200 kb plasmid simulation. The positioning of a plasmid locus (green) and a chromosome locus (red) were represented. The velocity of movement of the loci along the longitudinal axis of the nucleoid is measured for crossing events of the plasmid (orange lines) and the chromosome (black lines). The average velocity of the detected crossing events was plotted. F) Distribution of mobility of plasmid

loci at the polar position (longitudinal position <500 nm or >1500 nm). The 3D displacement of the locus is measured for intervals of 15 000 iteration.

Figure 5. A) Examples of the localization of the *parS*/ParB-GFP foci (green) at the Ori-7 position of the chromosome (top) and on a 137 kb excised circle (bottom). The nucleoid is labeled with the HU-mCherry fusion (red). The positioning of *parS*/ParB-GFP foci according to cell size were recorded before or 1h after induction of the Xis and Int recombinase to promote excision. B) Kymographs representing the movement of *parS*/ParB-GFP foci at the chromosomal locus, on the excised circle, R27 and R27 Δ*parAB* plasmids. Duration and frame intervals are indicated on top of each kymograph. C) Montage of a representative ballistic movement of the excised circle. D) Mean Squared Displacement analysis of *parS*/ParB-GFP focus at the chromosomal location or on the 137 kb excised circle. E) Log –Log representation of the MSD analysis presented in D. Power law fitting of the data $MSD=D*\Delta T^{\alpha}$. F) Mean Squared Displacement analysis of *parS*/ParB-GFP focus on the R27 and R27 ΔparAB plasmids. E) Log –Log representation of the MSD analysis presented in F Power law fitting of the data $MSD=D*\Delta T^{\alpha}$.

Figure 6. A) Average normalized fluorescence intensity of *parS*/ParB-GFP foci on excised circles and nucleoid labeled with HU-mCherry along the longitudinal axis of the cell. Cell border is determined as the half maximum of the phase contrast signal. B) Lateral and longitudinal displacements (60 x 120 sec) of an excised *parS*/ParB-GFP focus at the nucleoid edge. The nucleoid (red shade) is drawn for illustration, its exact contour changes from frame to frame. C) 3D timelapse imaging of the movement of excised foci at the edge of the nucleoid. Imaging was of *parS*/ParB-GFP and HU-mCherry was performed with 5 Z planes (interval 200 nm each) at 20 second intervals. Images were deconvoluted and 3D reconstructed. D) Examples of the localization of the *parS*/ParBGFP foci (green) on a 137 kb excised circle in the presence of chloramphenicol to condense the nucleoid (HU-mCherry, Red). The arrow indicates the movement of excised foci toward lateral edges of the nucleoid. Right panel, kymograph along the longitudinal axis of the cell marked with the arrow. E) Same as in A with a shorter imaging time interval (6 sec). Movement of excised foci toward lateral edges of the nucleoid is also observable at this time scale. Kymograph (along the white line) showing the movement of the polar *parS*/ParB-GFP foci toward the cell center via nucleoid edges. F) Localization of the R27 and R27 and R27 *ΔparAB* in the presence of chloramphenicol. G) Examples of the localization of the *parS*/ParBGFP foci (green) on a 137 kb excised circle in the presence of cephalexin to block division and create large cytoplasmic regions in between nucleoids (HU-mCherry, Red). The arrow on the right panel indicates the only *parS*/ParB-GFP focus crossing the cytoplasmic space observed among 200 cells. H) Examples of the localization of the parS/ParBGFP foci (green) on a 137 kb excised circle in the presence of rifampicin to decondense nucleoids (HU-mCherry, Red). I) Timelapse (360 sec with 6 sec intervals) of dynamics of excised foci in the presence of rifampicin (top); bottom Kymograph of the cell presented on the top panel.

Legend of the supplementary figures

Supplementary Figure S1. Measure of the rate of loss of R27, R27 Δ*parAB* and R27 Δ*parMR* plasmids

Supplementary Figure S2. A) Traces of the positioning along the longitudinal axis of the nucleoid of a 200 kb plasmid in the presence (green dots) or absence of chromosome (blue circles) within the

nucleoid. B) Distribution of the positioning of the 200 kb plasmid along the longitudinal axis of the nucleoid in the presence (green) or absence (orange) of the chromosome. C) Distribution of the positioning of the 200 kb plasmid along lateral axis of the nucleoid in the presence (green) or absence (orange) of the chromosome. D) Traces of the positioning along the longitudinal axis of the nucleoid of a 600 kb plasmid in the presence (green dots) or absence of chromosome (blue circles) within the nucleoid. E) Distribution of the positioning of the 600 kb plasmid along the longitudinal axis of the nucleoid in the presence (green) or absence (orange) of the chromosome. F) Distribution of the positioning of the 600 kb plasmid along lateral axis of the nucleoid in the presence (green) or absence (orange) of the chromosome.

Supplementary Figure S3. A) Distribution of the 200kb plasmid spatial extension along the longitudinal axis of the nucleoid according to the positioning of its barycenter in the presence of a chromosome. B) Distribution of the 200kb plasmid spatial extension along the longitudinal axis of the nucleoid according to the positioning of its barycenter in the absence of a chromosome. C) Distribution of the 200kb plasmid spatial extension along the lateral axis of the nucleoid according to the positioning of its barycenter in the presence of a chromosome. B) Distribution of the 200kb plasmid spatial extension along the lateral axis of the nucleoid according to the positioning of its barycenter in the absence of a chromosome.

Table S1 : Annotation of segregation systems for 973 plasmids from enterobacteria

TableS2: Plasmid count per genus

Table S3: Plasmids with no segregation systems

Text S1: HMM profile constructed using the conserved N-terminal domains of the StbA homologs detected.

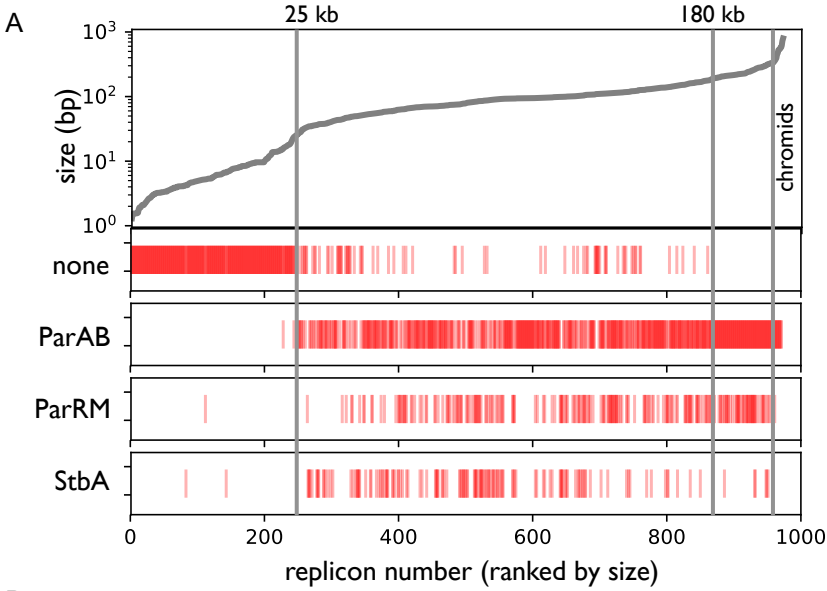
A
25 kb
180 kb
size (bp)
chromids
none
ParAB
ParRM
StbA
0
200
400
600
800
1000
replicon number (ranked by size)

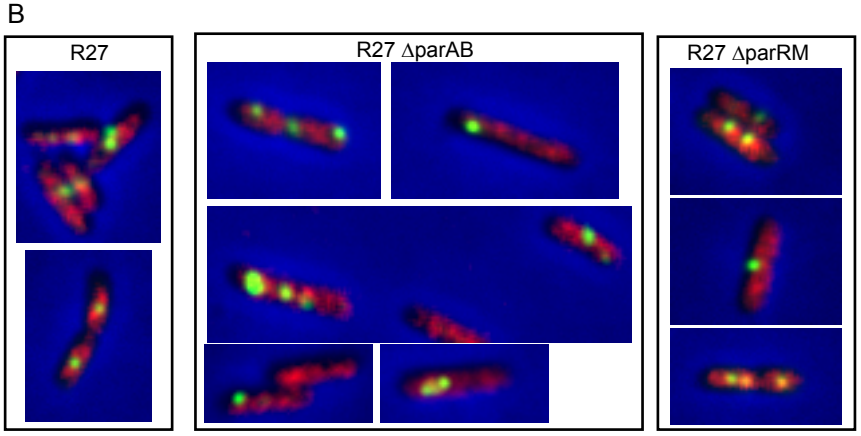
B
R27
R27 ΔparAB
R27 ΔparRM

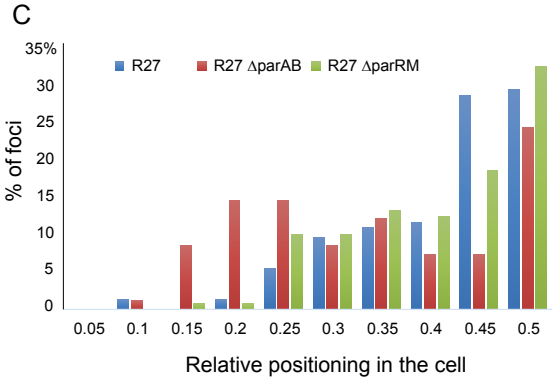
C
R27
R27 ΔparAB
R27 ΔparRM
% of foci
Relative positioning in the cell

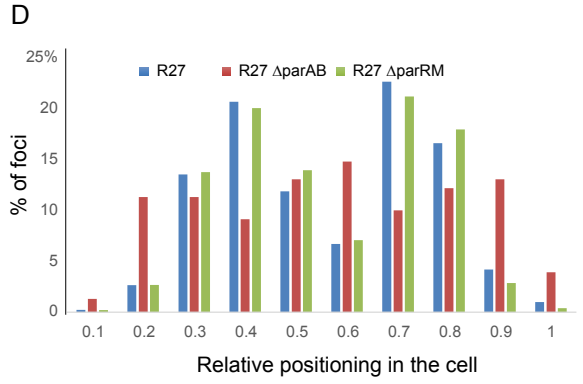
D
R27
R27 ΔparAB
R27 ΔparRM
% of foci
Relative positioning in the cell

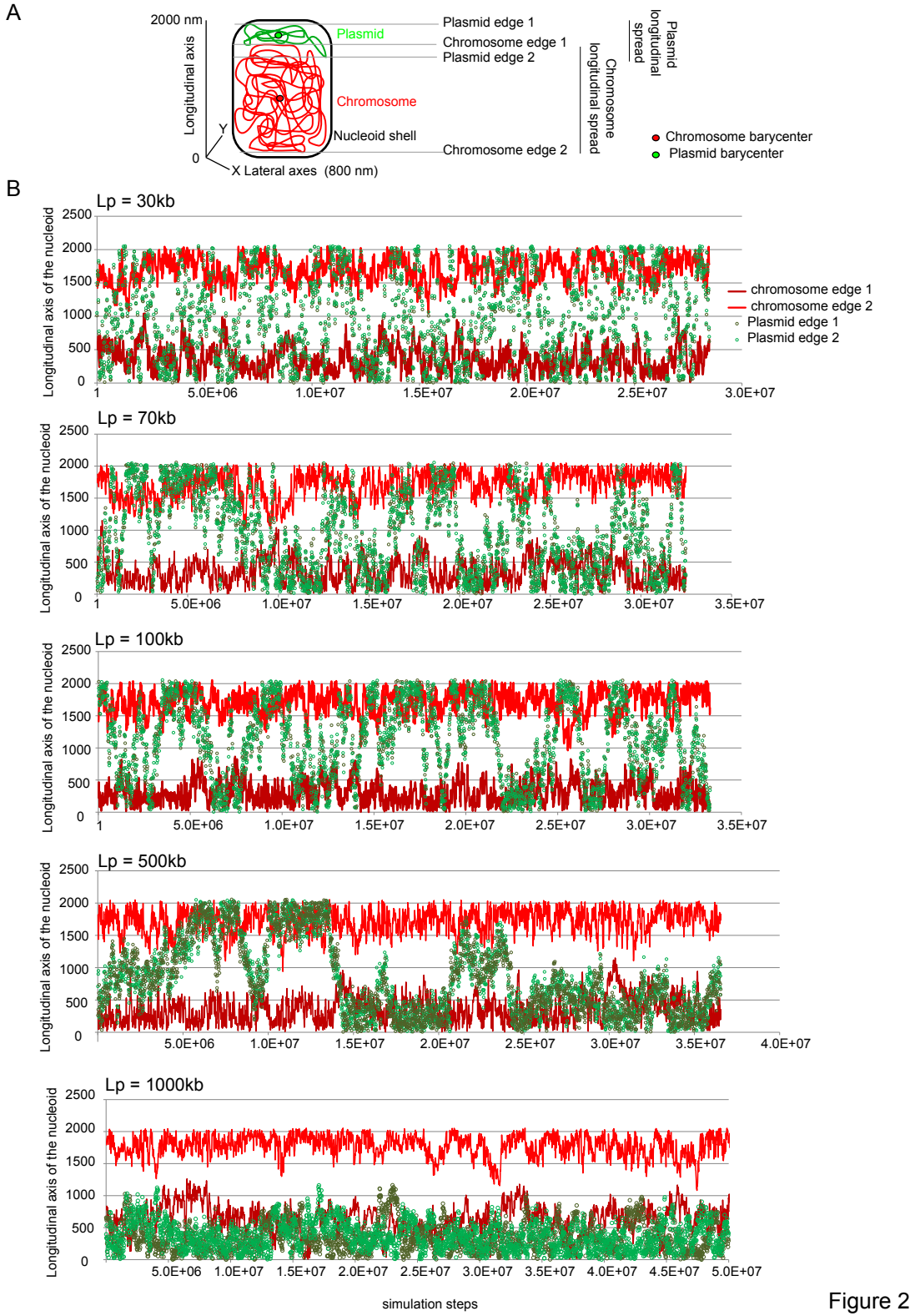
A
2000 nm
Longitudinal axis
Y
0
X Lateral axes (800 nm)
Plasmid
Chromosome
Nucleoid shell
Plasmid edge 1
Chromosome edge 1
Plasmid edge 2
Chromosome edge 2
Chromosome longitudinal spread
Plasmid longitudinal spread
Chromosome barycenter
Plasmid barycenter
B
Lp = 30kb
Lp = 70kb
Lp = 100kb
Lp = 500kb
Lp = 1000kb
Longitudinal axis of the nucleoid
chromosome edge 1
chromosome edge 2
Plasmid edge 1
Plasmid edge 2
simulation steps

Figure 2

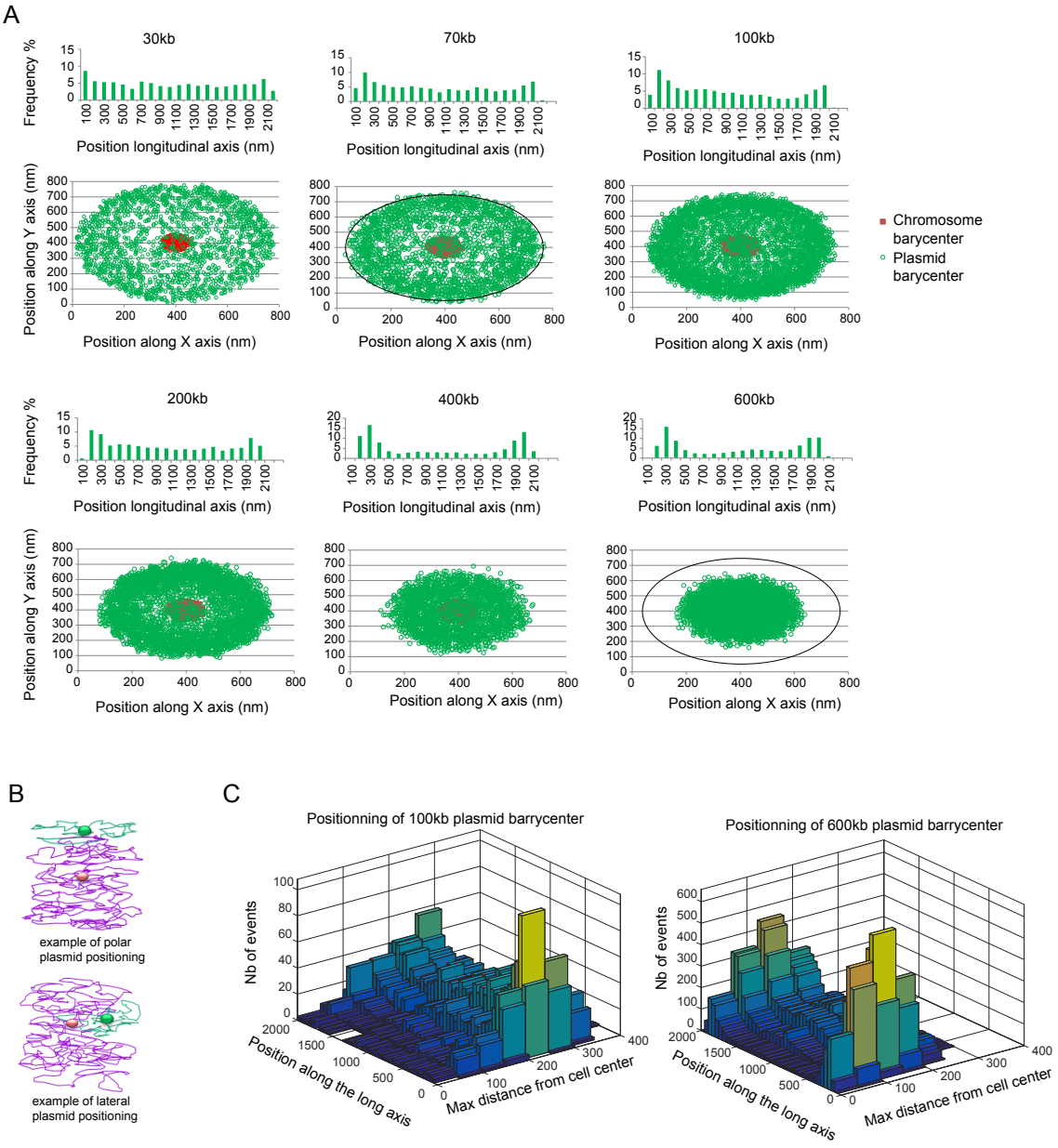
A
30kb
70kb
100kb
200kb
400kb
600kb
Frequency %
Position longitudinal axis (nm)
Position along Y axis (nm)
Position along X axis (nm)
Chromosome barycenter
Plasmid barycenter
B
example of polar plasmid positioning
example of lateral plasmid positioning
C
Positionning of 100kb plasmid barrycenter
Positionning of 600kb plasmid barrycenter
Nb of events
Position along the long axis
Max distance from cell center

Figure 3

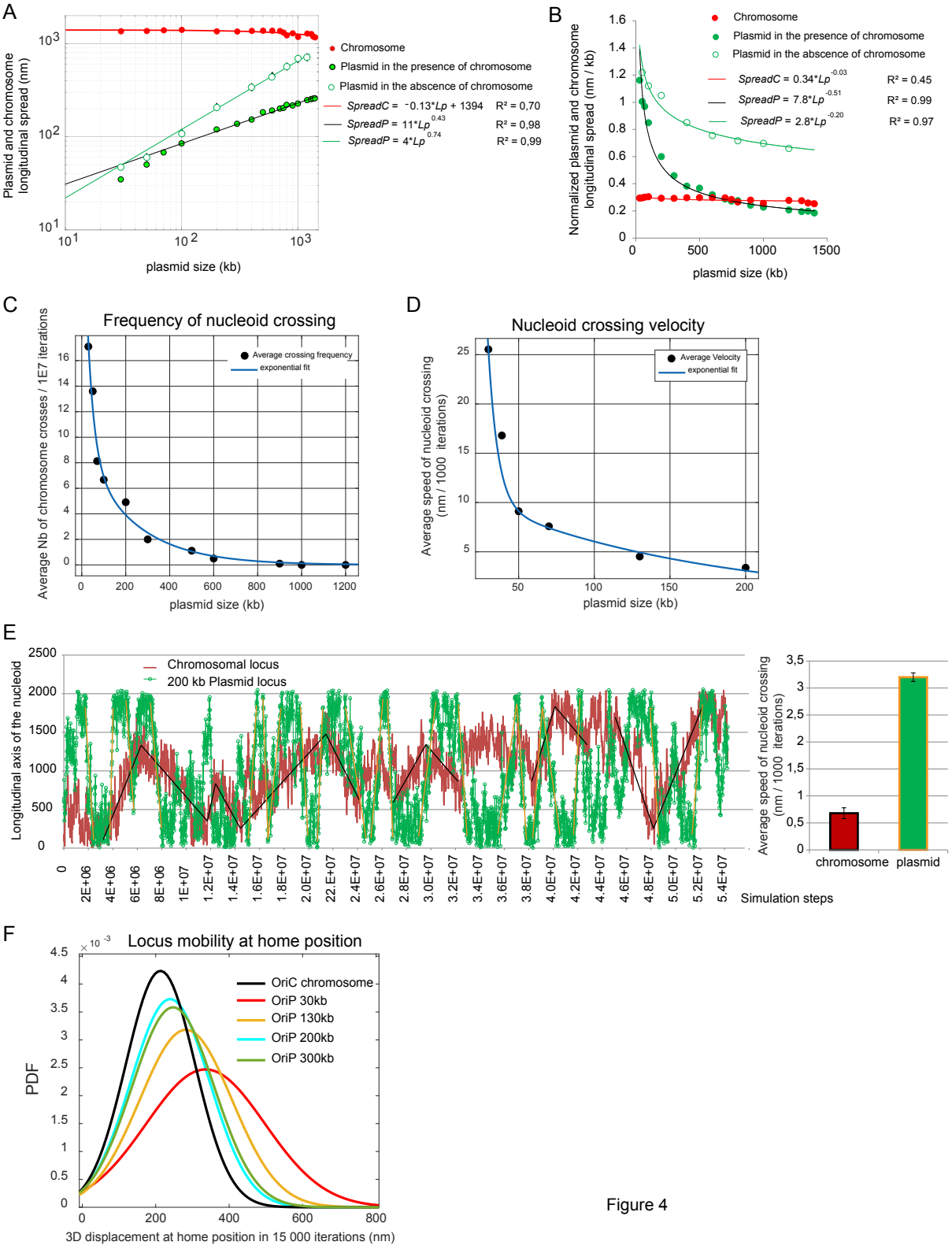
A
Plasmid and chromosome longitudinal spread (nm)
plasmid size (kb)
Chromosome
Plasmid in the presence of chromosome
Plasmid in the abscence of chromosome
SpreadC = -0.13*Lp + 1394 R² = 0,70
SpreadP = 11*Lp^0.43 R² = 0,98
SpreadP = 4*Lp^0.74 R² = 0,99
B
Normalized plasmid and chromosome longitudinal spread (nm / kb)
plasmid size (kb)
Chromosome
Plasmid in the presence of chromosome
Plasmid in the abscence of chromosome
SpreadC = 0.34*Lp^-0.03 R² = 0.45
SpreadP = 7.8*Lp^-0.51 R² = 0.99
SpreadP = 2.8*Lp^-0.20 R² = 0.97
C
Frequency of nucleoid crossing
Average Nb of chromosome crosses / 1E7 iterations
plasmid size (kb)
Average crossing frequency
exponential fit
D
Nucleoid crossing velocity
Average speed of nucleoid crossing (nm / 1000 iterations)
plasmid size (kb)
Average Velocity
exponential fit
E
Longitudinal axis of the nucleoid
Chromosomal locus
200 kb Plasmid locus
Simulation steps
Average speed of nucleoid crossing (nm / 1000 iterations)
chromosome
plasmid
F
Locus mobility at home position
PDF
OriC chromosome
OriP 30kb
OriP 130kb
OriP 200kb
OriP 300kb
3D displacement at home position in 15 000 iterations (nm)

Figure 4

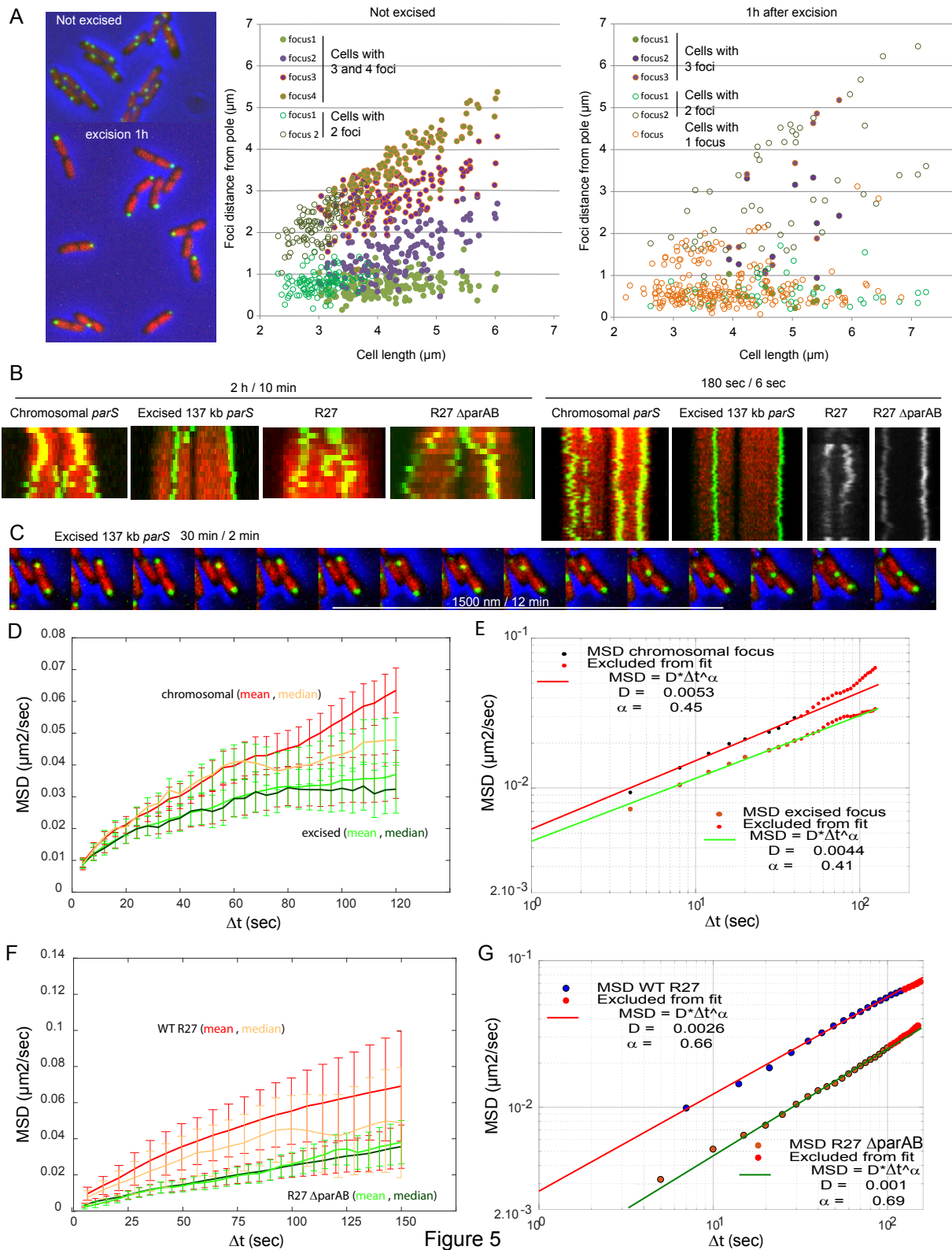
A
Not excised
excision 1h
Not excised
Foci distance from pole (µm)
Cell length (µm)
focus1
focus2
focus3
focus4
Cells with
3 and 4 foci
focus1
focus 2
Cells with
2 foci
1h after excision
Foci distance from pole (µm)
Cell length (µm)
focus1
focus2
focus3
Cells with
3 foci
focus1
focus2
Cells with
2 foci
focus
Cells with
1 focus
B
2 h / 10 min
Chromosomal parS
Excised 137 kb parS
R27
R27 ΔparAB
180 sec / 6 sec
Chromosomal parS
Excised 137 kb parS
R27
R27 ΔparAB
C
Excised 137 kb parS 30 min / 2 min
1500 nm / 12 min
D
MSD (µm2/sec)
chromosomal (mean , median)
excised (mean , median)
Δt (sec)
E
MSD chromosomal focus
Excluded from fit
MSD = D*Δt^α
D = 0.0053
α = 0.45
MSD excised focus
Excluded from fit
MSD = D*Δt^α
D = 0.0044
α = 0.41
MSD (µm2/sec)
Δt (sec)
F
MSD (µm2/sec)
WT R27 (mean , median)
R27 ΔparAB (mean , median)
Δt (sec)
G
MSD WT R27
Excluded from fit
MSD = D*Δt^α
D = 0.0026
α = 0.66
MSD R27 ΔparAB
Excluded from fit
MSD = D*Δt^α
D = 0.001
α = 0.69
MSD (µm2/sec)
Δt (sec)

Figure 5

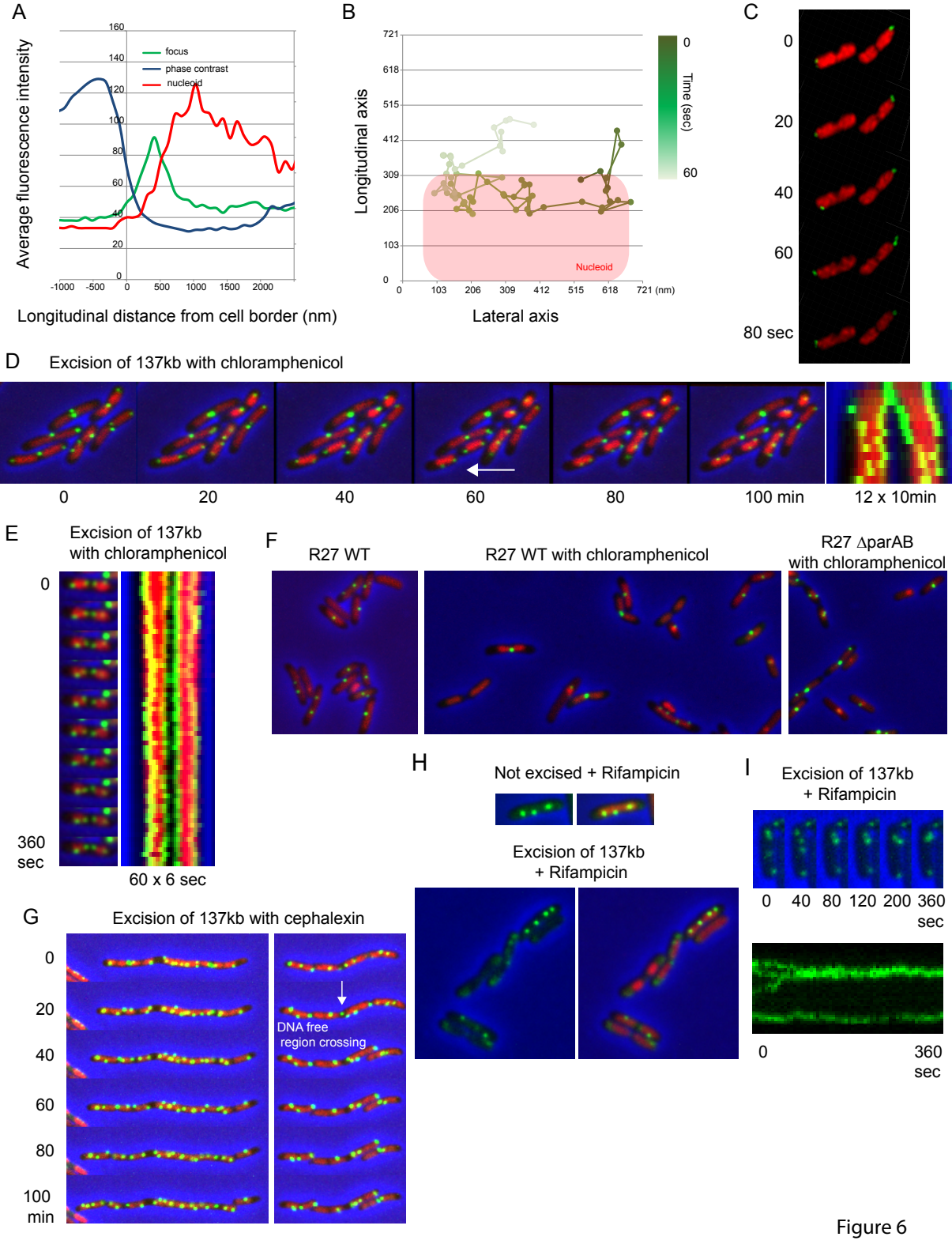
A
Average fluorescence intensity
focus
phase contrast
nucleoid
Longitudinal distance from cell border (nm)
B
Longitudinal axis
Time (sec)
Nucleoid
Lateral axis
C
0
20
40
60
80 sec
D
Excision of 137kb with chloramphenicol
0
20
40
60
80
100 min
12 x 10min
E
Excision of 137kb with chloramphenicol
0
360 sec
60 x 6 sec
F
R27 WT
R27 WT with chloramphenicol
R27 ΔparAB with chloramphenicol
G
Excision of 137kb with cephalexin
0
20
40
60
80
100 min
DNA free region crossing
H
Not excised + Rifampicin
Excision of 137kb + Rifampicin
I
Excision of 137kb + Rifampicin
0 40 80 120 200 360 sec
0
360 sec

Figure 6